Article

X-ray Opaque Polymer Drug-Eluting Beads Loaded with Iodized Oil: Preparation and In Vitro and In Vivo Evaluations

Jin Long Zhang,* Bing Yuan, Xiao Wei Zhang, Heng Zhang, Hao Wang, Xing Zhi Wang, and Hong Wei Zhao

Read Online

ACCESS | Metrics & More | Article Recommendations

ABSTRACT: Drug-eluting microspheres are commonly used as a local drug delivery system for interventional therapy. However, current drug-eluting microspheres have poor X-ray visibility, which can hinder tracking and postembolization evaluation. In the current study, X-ray-visible poly(acrylic acid) drug-eluting beads loaded with iodized oil (IO-PAA-DEBs) ranging from 100−300 μm were prepared and evaluated both in vitro and in vivo. Iodized oil served as the radiopaque agent, and X-ray and computed tomography scanning confirmed that the microspheres exhibited excellent X-ray-visible properties. The drug-loading capacities of bleomycin hydrochloride, doxorubicin hydrochloride, and oxaliplatin were also investigated. IO-PAA-DEBs exhibited sustained drug release properties, accompanied by a cumulative drug release rate that reached approximately 60% after 120 h. In vitro and in vivo experiments revealed that IO-PAA-DEBs had good biocompatibility. Collectively, these results demonstrated that IO-PAA-DEBs could facilitate transarterial embolization and sustained drug delivery.
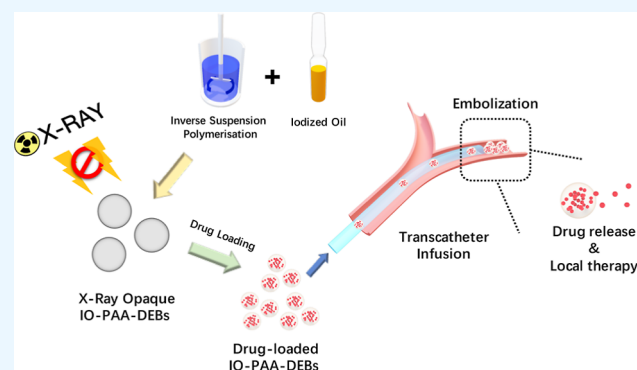
1. INTRODUCTION

Interventional therapy guided by digital subtraction angiography has been widely used in the diagnosis and treatment of vascular diseases and tumors.[1,2] Interventional therapies, such as transcatheter arterial chemoembolization, endovascular stent implantation, thrombus removal, and ablation therapy, are minimally invasive procedures with high safety and efficacy.[1,3−6]

Microspheres are spherical, micrometer-sized spheres with a wide range of applications in medical and industrial fields.[4,7,8] Importantly, microspheres exhibit unique physicochemical properties, including specific surface area, porosity, and surface reactivity, which make them attractive for numerous applications, particularly for those related to drug delivery and interventional therapies. Drug-loaded microspheres, also called drug-eluting beads (DEBs),[9] are typically employed to deliver chemotherapeutic drugs directly to the tumor site, leading to tumor cell death and suppressed tumor growth due to chemotherapeutic toxicity, local ischemia, and necrosis.[10,11] Microsphere-loaded drugs can be released continuously at the embolized site at a relatively slow rate, thus killing tumor cells over a prolonged period.

To better embolize blood vessels and transport drugs, DEBs are designed as spherical, porous particles with diameters ranging from 100 to 300 μm.[12−14] However, most materials used to prepare DEBs are low-density organic polymers, which render them radiolucent, leading to an inaccurate assessment of the embolization range via X-ray imaging.

In the current study, X-ray-imageable poly(acrylic acid) (PAA)-DEBs loaded with iodized oil (IO-PAA-DEBs) were prepared and evaluated both in vitro and in vivo. Three kinds of therapeutics, doxorubicin (DOX), bleomycin hydrochloride (BLM), and oxaliplatin (OXA), were used to investigate maximum drug loading and in vitro drug release, and their pharmacokinetic profiles were assessed. Furthermore, surface characterization, X-ray-visible properties, and biocompatibility were evaluated.

2. MATERIALS AND METHODS

2.1. Materials. Acrylic acid, N,N'-methylenebis (2-propenamide), ammonium persulfate, and n-heptane were purchased from Shanghai Macklin Biochemical Co. Ltd. (Shanghai, China); poly(vinyl alcohol) 1788 (PVA-1788), paraffin liquid, and N,N,N',N'-tetramethylethylenediamine (TEMED) were purchased from Shanghai Aladdin Biochem-
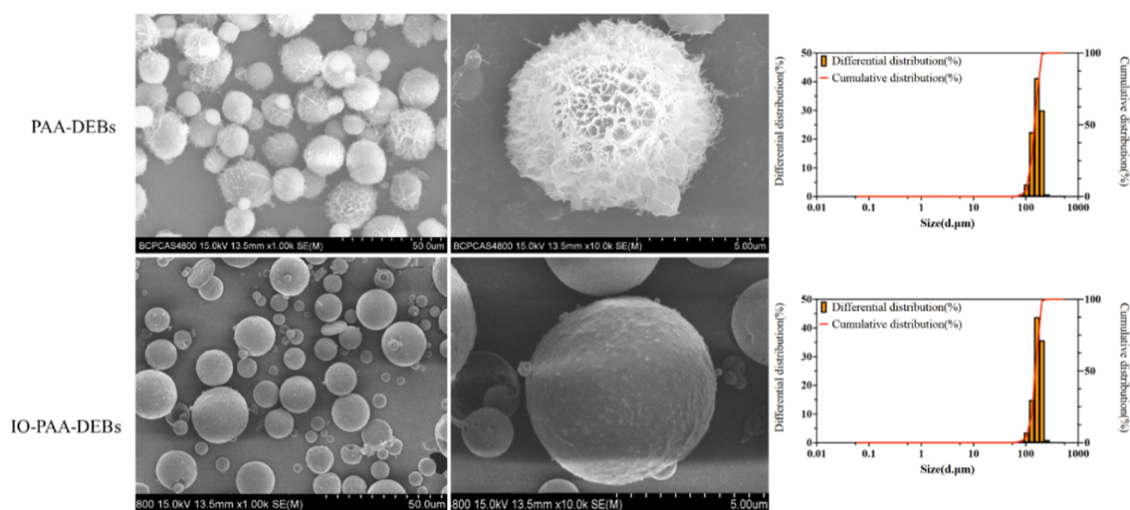
Figure 1. SEM results and size distributions of PAA-DEBs and IO-PAA-DEBs. PAA-DEBs and IO-PAA-DEBs were freeze-dried to remove water, surface-coated with gold, and then observed and photographed using SEM (the grayscale images on the left side). The particle size distributions of both PAA-DEBs and IO-PAA-DEBs are similar, with good uniformity (the column graphs on the right side). SEM, scanning electron microscopy; PAA-DEBs, poly(acrylic acid) drug-eluting beads; IO-PAA-DEBs, poly(acrylic acid) drug-eluting beads loaded with iodized oil.

ical Technology Co. Ltd. (Shanghai, China); Span 80 was purchased from Sigma-Aldrich (St. Louis, MO, USA); lipiodol ultra fluid was purchased from Guerbet, LLC (Princeton, NJ, USA); DOX and OXA were purchased from Energy Chemical (Shanghai, China); and BLM was purchased from GlpBio Technology (Montclair, CA, USA).

2.2. Preparation of PAA-DEBs and IO-PAA-DEBs. PAA-DEBs and IO-PAA-DEBs were prepared by using inverse suspension polymerization. Liquid paraffin (50 mL) containing 0.5% Span 80 was used as the oil phase. The oil phase was stirred at 500 rpm magnetic stirring and preheated to 55 °C. The aqueous phase comprised 0.5 g of methylene bis-(acrylamide), 2.0 g of ammonium persulfate, 5.0 g of acrylic acid, 0.5 g of PVA-1788, and 5.5 g of water. Regarding IO-PAA-DEBs, lipiodol ultra fluid (0 or 1.0 g) was added and premixed in the aqueous phase as the contrast agent. Under nitrogen protection, the aqueous phase was added dropwise into the preheated oil phase, and the mixture was stirred for 10 min to form a suspension. Then, 500 μL of TEMED was added into the suspension to trigger polymerization. After further stirring for 1 h, microspheres with particle sizes of 100−300 μm were collected and washed with *n*-heptane. PAA-DEBs and IO-PAA-DEBs were freeze-dried to remove water.

2.3. Surface Characterization of PAA-DEBs and IO-PAA-DEBs. A laser particle size analyzer was used to determine the size distribution of the DEBs. Scanning electron microscopy (SEM) was performed to examine the morphologies of PAA-DEBs and IO-PAA-DEBs. The samples were coated with gold using a sputter coater prior to SEM imaging.

2.4. Drug-Loading Capacity. Aqueous solutions of DOX, BLM, and OXA were prepared separately. The dried IO-PAA-DEBs (0.1 g) were completely immersed in each drug solution. The mixture was stirred vigorously at 50 rpm and 20 °C. The microspheres were collected and washed three times with purified water at predetermined time points. The drug content of the microspheres was quantified by using high-performance liquid chromatography (HPLC). The maximum drug-loading content was evaluated. All procedures were performed under light-protected conditions and repeated in triplicate.

2.5. In Vitro Drug Release. In vitro simulated release experiments were conducted to investigate the sustained-release capability of the IO-PAA-DEBs. Initially, DOX, BLM, and OXA were maximally loaded into IO-PAA-DEBs (50 mg), followed by shaking at 50 rpm in 50 mL of the simulated pH 7.4 phosphate-buffered saline (PBS) at 25 or 37 °C using a constant-temperature shaker. At predetermined intervals, the release medium (0.5 mL) was quantitatively removed, and HPLC was used to calculate the cumulative drug release. Fresh release medium was immediately replenished after each sampling. All operations were conducted under light-avoiding conditions, and measurements were performed in triplicate.

2.6. Cytotoxicity Test. The PAA-DEBs or IO-PAA-DEBs (50 mg) were soaked in pH 7.4 PBS, followed by placement in a constant-temperature shaker at 50 rpm and 37 °C. The supernatant was collected, filtered at predetermined time points, and stored at −20 °C for later use. The 293T cells were cultured in DMEM complete medium in a cell culture incubator under 5% CO_2 at 37 °C. Upon reaching the logarithmic growth phase, cells were seeded in a 96-well plate at a density of 7000 cells/well. The DEB eluent was sequentially added into a 96-well plate, and the cells were further cultured for 24−72 h. Cell viability and growth inhibition rates were measured using the CCK-8 assay to evaluate the biocompatibility of the prepared DEBs.

2.7. Animals. Three male Wistar rats (body weight 200 ± 10 g) were maintained in cages at 18−22 °C under controlled humidity (55 ± 6%) and a 12 h light−dark cycle and were provided standard laboratory food and water. Three adult male beagle dogs (mean age, 1.9 years ± 0.1; range, 1.8−2.0 years; mean weight, 11.2 kg ± 1.1; range, 10.0−12.2 kg) were castrated under general anesthesia, and a benign prostatic hyperplasia model was established using hormone therapy as described previously.[15] All animals were allowed to adapt for 1 week prior to the experiment.

2.8. Ethical Approval. All animal experiments were approved by the Institutional Animal Research Ethics Committee of Chinese PLA General Hospital (SQ2020013) and complied with institutional animal care guidelines.
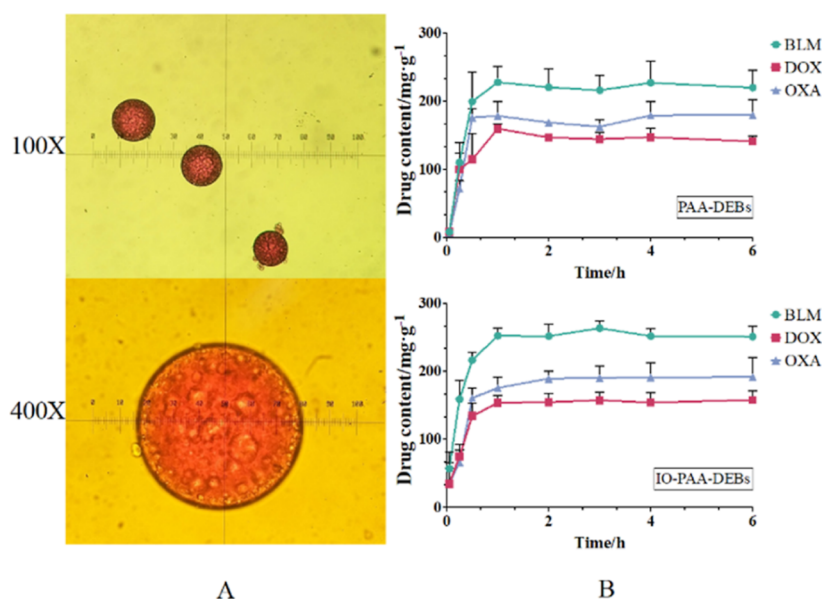
Figure 2. Photomicrographs and drug loading−time profiles of IO-PAA-DEBs. (A) Images of DOX-loaded IO-PAA-DEBs observed using an optical microscope. (B) Drug-loading curves of IO-PAA-DEBs. Mean ± standard deviation (SD), n = 3. BLM, bleomycin hydrochloride; DOX, doxorubicin hydrochloride; OXA, oxaliplatin; IO-PAA-DEBs, poly(acrylic acid) drug-eluting beads loaded with iodized oil.

2.9. In Vivo X-ray Visibility.

To verify the in vivo radiopacity of IO-PAA-DEBs, three Wistar rats were anesthetized and administered PAA-DEBs or IO-PAA-DEBs (0.1 g of DEBs suspended in 1 mL of purified water) via intramuscular injection in both femoral muscles. Real-time X-ray and computed tomography (CT) scans were used to evaluate X-ray visibility.

2.10. In Vivo Embolization and Biocompatibility.

The benign prostatic hyperplasia model was successfully established in all three adult male beagle dogs. Subsequently, prostatic artery embolization (PAE) was performed using IO-PAA-DEBs under general anesthesia, as described in our previous study;[15] only the right or left hemiprostate was embolized. A noncontrast CT scan was performed to assess the DEB radiopacity and distribution in the prostate immediately post-PAE. All three dogs were euthanized under anesthesia by administering an intravenous injection of potassium chloride 48 h post-PAE. The prostates were harvested, fixed in a 4% formaldehyde solution, and embedded in paraffin. Then, sections were stained by using hematoxylin and eosin (H&E) to assess the distribution and irritative effect of IO-PAA-DEBs at the embolization site.

2.11. Statistical Analysis.

Data were analyzed using GraphPad Prism (9.0.1; GraphPad, San Diego, CA, USA). The experimental results were analyzed using a one-way ANOVA test for multiple-group analysis, and $p < 0.05$ was considered statistically significant.

3. RESULTS AND DISCUSSION

3.1. Morphology and Size Distribution.

Figure 1 illustrates the SEM images and size distribution results for PAA-DEBs and IO-PAA-DEBs. The microspheres prepared without iodized oil were spherical and exhibited a porous structure, with pore sizes ranging from 0.5 to 1.0 μm. IO-PAA-DEBs were also spherical but had a relatively smooth surface, without visible pore-like structures, as the iodized oil functioned as a filling agent. PAA formed a porous skeleton structure in the DEBs, and the addition of iodized oil resulted

in a smoother IO-PAA-DEB surface. PAA-DEBs and IO-PAA-DEBs exhibited similar particle size distributions, with D50 values of 147.83 and 154.04 μm, respectively. This indicates that the addition of lipiodol exerted a negligible effect on the particle size of the DEBs.

3.2. Drug-Loading Capacity.

The drug-loading profiles are shown in Figure 2. For observation under an optical microscope, DOX was selected as the model drug owing to its red appearance in an aqueous solution. According to optical microscopy images (Figure 2A), IO-PAA-DEBs remained circular and exhibited clear red coloration, indicating that the drug was effectively loaded. Figure 2B presents the relationship between the drug loading and time. PAA-DEBs and IO-PAA-DEBs exhibited similar drug-loading characteristics, with the maximum loading value reaching approximately 1 h. IO-PAA-DEBs had a higher maximum drug-loading capacity than that of PAA-DEBs, which could be attributed to the filling effect of the iodized oil, leading to smaller pores on the surfaces of the DEBs and less drug loss during washing. Figure 3 presents the morphology and average size of IO-PAA-DEBs in dry, wet, and drug-loaded (wet) states. In the wet state (drug-loaded or unloaded), the average particle size of IO-PAA-DEBs was approximately 150 μm, which was significantly larger than that
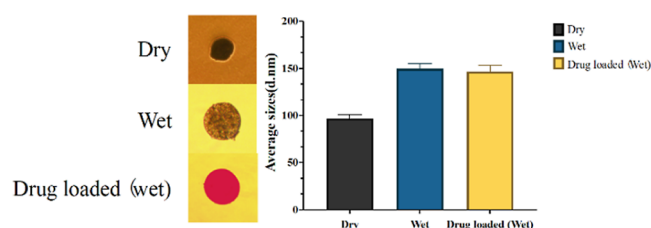

Figure 3. Shapes and average sizes of the dry, wet, and drug-loaded IO-PAA-DEBs. DOX was used as the model drug (red color in the left picture). The particle size of IO-PAA-DEBs increases significantly upon drug loading or hydration (the right bar chart). DOX, doxorubicin hydrochloride; IO-PAA-DEBs, poly(acrylic acid) drug-eluting beads loaded with iodized oil.
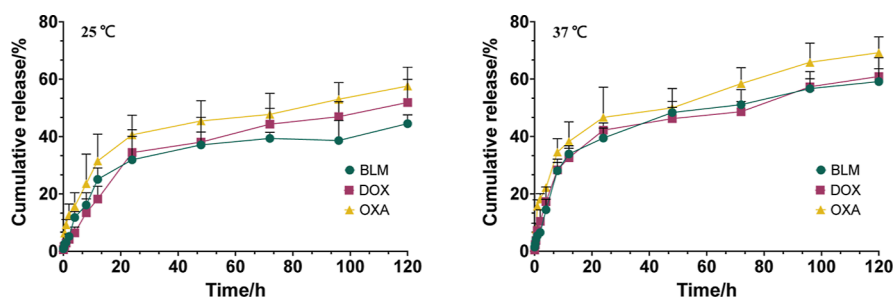
Figure 4. In Vitro cumulative drug release in PBS (pH 7.4). Mean ± SD, $n = 3$. BLM, bleomycin hydrochloride; DOX, doxorubicin hydrochloride; OXA, oxaliplatin.
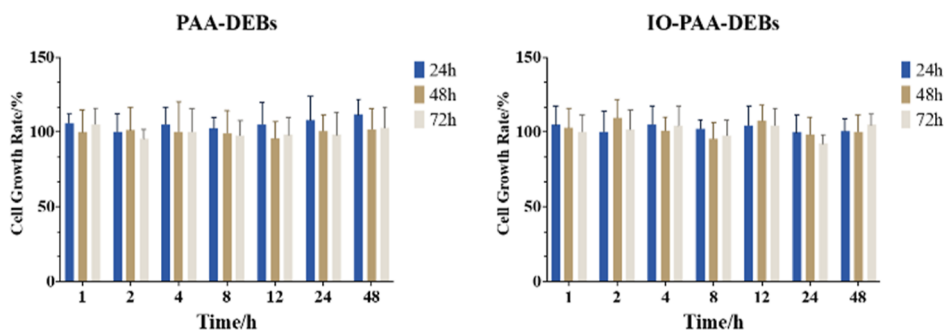

Figure 5. Cell growth rate results for PAA-DEBs and IO-PAA-DEBs. Mean ± SD, $n = 6$. PAA-DEBs, poly(acrylic acid) drug-eluting beads; IO-PAA-DEBs, poly(acrylic acid) drug-eluting beads loaded with iodized oil.
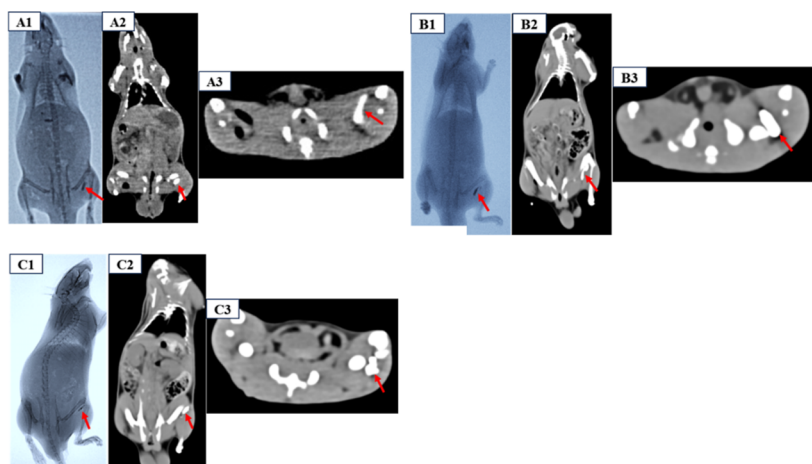

Figure 6. X-ray and CT imaging results of PAA-DEBs and IO-PAA-DEBs injected in rats (A−C). (A1−C1) X-ray imaging of PAA-DEBs (left) and IO-PAA-DEBs (right), IO-PAA-DEBs with significant radiopacity (red arrow); (A2−C2): CT image showing the injection site of IO-PAA-DEBs (red arrow) on coronal view; (C) CT image showing the injection site of IO-PAA-DEBs (red arrow) on axial view. CT, computed tomography; PAA-DEBs, poly(acrylic acid) drug-eluting beads; IO-PAA-DEBs, poly(acrylic acid) drug-eluting beads loaded with iodized oil.

in the dry state, indicating a swelling process upon water absorption. Moreover, PAA carries a certain amount of negative charge; therefore, IO-PAA-DEBs may undergo drug loading via a combined mechanism of swelling and ion exchange.

3.3. In Vitro Drug Release. Figure 4 presents the results of the in vitro drug release of IO-PAA-DEBs loaded with different therapeutics. At 37 °C, the drug release process was divided into two phases: the first phase occurred within 20 h, during which approximately 40% of the drug was rapidly released from the DEBs. Subsequently, the drug release rate decreased, and the cumulative drug release rate reached approximately 60% at 120 h. All three model drugs exhibited similar effects. At 25 °C, drug release was slower than at 37 °C,

although the overall trend remained the same. This drug release behavior aligns with characteristics typically associated with microsphere-type formulations, where drugs residing on the surface or outer layer of DEBs tend to be released more quickly than those present within DEBs, which are constrained by the structural framework and, consequently, released less rapidly. This drug release pattern could enable the drug concentration within the embolized area to rapidly reach the therapeutic window, thereby enhancing the duration of drug action and augmenting the therapeutic efficacy.

3.4. Cytotoxicity Test. Figure 5 illustrates the cell proliferation rates. Based on the findings, the eluate collected from the DEBs at various time points did not exhibit significant cytotoxicity toward the 293T cells, indicating that the DEBs
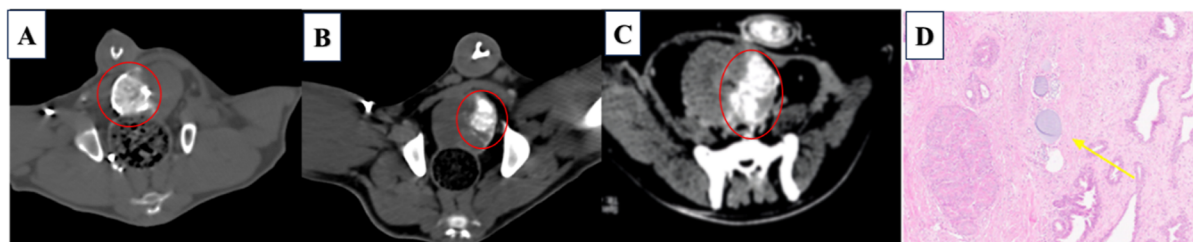
Figure 7. CT scan and H&E results of prostate embolization in beagle dogs. (A) Noncontrast CT scan of the axial view of the prostate showing IO-PAA-DEB deposition in the right hemiprostate (circle); (B,C) IO-PAA-DEB deposition in the left hemiprostate (circle); (D) H&E staining of the prostate shows microspheres (yellow arrow) embolized in the vessels (100×), with the integrity of the vessel wall maintained without inflammatory cell infiltration. CT, computed tomography; H&E, hematoxylin and eosin; IO-PAA-DEBs, poly(acrylic acid) drug-eluting beads loaded with iodized oil.

did not release any deleterious chemicals capable of cell damage in the aqueous medium, thereby demonstrating excellent biocompatibility.

3.5. X-ray Visibility. According to X-ray and CT scan images, PAA-DEBs had negligible radiopacity, whereas IO-PAA-DEBs had significant radiopacity (Figure 6A–C). As shown in Figure 6A–C, the IO-PAA-DEBs remained at the injection site and were radiopaque upon X-ray and CT imaging, which enabled differentiation from the surrounding normal tissues. Conversely, the PAA-DEBs exhibited negligible radioactivity and were not visible in vivo.

3.6. In Vivo Embolization and Biocompatibility. Figure 7A–C presents CT images of the prostate embolization procedure in the canine model using IO-PAA-DEBs. The noncontrast CT scan of the prostate revealed IO-PAA-DEB deposition in the prostate, with a high degree of radiopacity. Histological examination of H&E-stained sections revealed the presence of IO-PAA-DEBs within the embolized prostate vasculature, exhibiting intact vessel walls without any signs of inflammatory cell infiltration (Figure 7D), thereby suggesting that the IO-PAA-DEBs had good biocompatibility.

4. CONCLUSIONS

In this study, IO-PAA-DEBs were prepared and evaluated both in vitro and in vivo. BLM, DOX, and OXA were selected to determine the drug-loading capacity, revealing that IO-PAA-DEBs sustained excellent drug-loading capacities and release properties. In vitro and in vivo studies demonstrated that drug-loaded IO-PAA-DEBs exhibited good biocompatibility. Furthermore, owing to their excellent X-ray-visible properties, IO-PAA-DEBs could be used for the transarterial embolization of solid tumors, allowing the accurate distribution of DEBs to evaluate the embolization efficacy in a timely manner and prevent nontarget embolization.

■ AUTHOR INFORMATION

Corresponding Author

Jin Long Zhang − *Capital Medical University Affiliated Beijing Tongren Hospital Department of Radiology, Beijing 100730, China;* ⊙ orcid.org/0000-0003-3158-2130; Email: along0312@126.com

Authors

Bing Yuan − *Department of Interventional Radiology, Chinese PLA General Hospital, Beijing 100853, P. R. China*
Xiao Wei Zhang − *Hubei University, Wuhan 430062, China*

Heng Zhang − *Department of Radiology, Chinese PLA General Hospital Second Medical Center, Beijing 100853, China*
Hao Wang − *Shenyang Pharmaceutical University, Shenyang 117004, China*
Xing Zhi Wang − *Shenyang Pharmaceutical University, Shenyang 117004, China*
Hong Wei Zhao − *Capital Medical University Affiliated Beijing Tongren Hospital Department of Radiology, Beijing 100730, China*

Complete contact information is available at:
https://pubs.acs.org/10.1021/acsomega.3c09368

■ REFERENCES

(1) Delicque, J.; Boulin, M.; Guiu, B.; Pelage, J. P.; Escal, L.; Schembri, V.; Assenat, E.; Fohlen, A. Interventional oncology for hepatocellular carcinoma. *Clin. Res. Hepatol. Gastroenterol.* **2016**, *40* (5), 530−537.
(2) Öcal, O.; Rässler, D.; Ricke, J.; Seidensticker, M. Advances in diagnostic and interventional radiology in hepatocellular carcinoma. *Dig. Dis.* **2022**, *40* (4), 458−467.
(3) Sarno, G.; Montalti, R.; Giglio, M. C.; Rompianesi, G.; Tomassini, F.; Scarpellini, E.; De Simone, G.; De Palma, G. D.; Troisi, R. I. Hepatocellular carcinoma in patients with chronic renal disease: Challenges of interventional treatment. *Surg. Oncol.* **2021**, *36*, 42−50.
(4) Sheth, R. A.; Sabir, S.; Krishnamurthy, S.; Avery, R. K.; Zhang, Y. S.; Khademhosseini, A.; Oklu, R. Endovascular embolization by transcatheter delivery of particles: Past, present, and future. *J. Funct. Biomater.* **2017**, *8* (2), 12.
(5) Chang, Y.; Jeong, S. W.; Young Jang, J.; Jae Kim, Y. Recent updates of transarterial chemoembolilzation in hepatocellular carcinoma. *Int. J. Mol. Sci.* **2020**, *21* (21), 8165.
(6) Jiří, T.; Igor, K. Hepatocellular carcinoma future treatment options. *Klinicka Onkologie* **2020**, *33*, 26−29.
(7) Doucet, J.; Kiri, L.; O'Connell, K.; Kehoe, S.; Lewandowski, R. J.; Liu, D. M.; Abraham, R. J.; Boyd, D. Advances in degradable embolic microspheres: A state of the art review. *J. Funct. Biomater.* **2018**, *9* (1), 14.
(8) Itzhaki, E.; Elias, Y.; Moskovits, N.; Stemmer, S. M.; Margel, S. Proteinoid polymers and nanocapsules for cancer diagnostics, therapy and theranostics: In vitro and in vivo studies. *J. Funct. Biomater.* **2023**, *14* (4), 215.

(9) Facciorusso, A. Drug-eluting beads transarterial chemoembolization for hepatocellular carcinoma: Current state of the art. *World J. Gastroenterol.* **2018**, *24* (2), 161−169.

(10) Dasse, K. D.; Lander, M. J.; Novelli, P. M. Chemoembolization with drug-eluting beads for the treatment of hepatocellular carcinoma. *J. Adv. Pract. Oncol.* **2016**, *7* (7), 764−778.

(11) Raoul, J. L.; Forner, A.; Bolondi, L.; Cheung, T. T.; Kloeckner, R.; de Baere, T. Updated use of TACE for hepatocellular carcinoma treatment: How and when to use it based on clinical evidence. *Cancer Treat. Rev.* **2019**, *72*, 28−36.

(12) Binder, S.; Lewis, A. L.; Löhr, J. M.; Keese, M. Extravascular use of drug-eluting beads: A promising approach in compartment-based tumor therapy. *World J. Gastroenterol.* **2013**, *19*, 7586−7593.

(13) Woo, H. Y.; Heo, J. Transarterial chemoembolization using drug eluting beads for the treatment of hepatocellular carcinoma: Now and future. *Clin. Mol. Hepatol.* **2015**, *21* (4), 344−348.

(14) Lewis, A. L.; Willis, S. L.; Dreher, M. R.; Tang, Y.; Ashrafi, K.; Wood, B. J.; Levy, E. B.; Sharma, K. V.; Negussie, A. H.; Mikhail, A. S. Bench-to-clinic development of imageable drug-eluting embolization beads: Finding the balance. *Future Oncol.* **2018**, *14* (26), 2741−2760.

(15) Zhang, J. L.; Yuan, B.; Wang, M. Q.; Fu, J. X.; Duan, F.; Wang, T.; Shen, L.; Wang, Y.; Liu, J. H.; Shen, Y. G.; Wang, X. Q.; Zhang, H. T.; Li, H. W.; Yan, J. Y.; Song, Z. G. Prostatic artery embolization for benign prostatic hyperplasia: bleomycin-eluting versus bland microspheres in a canine model. *J. Vasc. Intervent. Radiol.* **2020**, *31* (5), 820−830.